Catal Lett (2008) 121:189–198
DOI 10.1007/s10562-007-9336-x

A Novel Combustion Synthesis Preparation of CuO/ZnO/ZrO_2/Pd for Oxidative Hydrogen Production from Methanol

Stephen Schuyten · Peter Dinka · Alexander S. Mukasyan · Eduardo Wolf

Received: 17 September 2007 / Accepted: 31 October 2007 / Published online: 5 December 2007

Abstract Complex catalysts containing combinations of copper, zinc, zirconium, and palladium oxides were prepared via three combustion synthesis routes including volume combustion, impregnated substrate combustion, and so-called second wave impregnation combustion methods. These catalysts were characterized via XRD, XPS, N_2O decomposition and BET techniques and evaluated for their activity and selectivity for the partial oxidation of methanol. The novel second combustion wave method showed superior palladium active metal loadings compared to conventional volume combustion synthesis modes. Palladium is also shown to significantly lower the reduction temperature of bulk CuO. Combustion synthesis based methods show promise for synthesis of methanol reforming catalysts.

Keywords Methanol partial oxidation · Copper · Palladium · Catalyst · Combustion synthesis

1 Introduction

Hydrogen has potential for use as a localized energy source to replace batteries inside electronic devices or to power vehicles. Proton-exchange membrane (PEM) fuel cells using hydrogen as fuel are efficient, quiet, and have near zero harmful emissions. Elemental hydrogen is not readily available, but it can be freed from sources such as methanol, natural gas, water, biomass, or other hydrocarbons [1–3]. Among these, methanol is attractive as a hydrogen carrier because it is an abundant commodity chemical that can be stored as a liquid at ambient temperatures.

Several different approaches exist for producing hydrogen from methanol including methanol decomposition (MD), steam reforming (SRM), partial oxidation (POM), and combined steam and oxidative reforming (CMR). Operation of PEM fuel cells that use precious metal catalysts such as platinum require hydrogen fuel which contains less than 50 ppm carbon monoxide to prevent catalyst poisoning. Therefore it is critical to select a hydrogen reforming method that minimizes carbon monoxide byproduct formation. Steam reforming has the highest hydrogen to carbon ratio but it is highly endothermic and not suitable for applications where a heat source is unavailable. Partial oxidation is an exothermic process with reduced tendency to form carbon monoxide and a higher reaction rate than SRM [4].

Copper based catalysts have been extensively used and studied for methanol synthesis, water gas shift (WGS), SRM, POM, and CMR reactions. For example, typical copper-based catalysts for methanol synthesis and reforming are paired with ZnO and/or Al_2O_3. Aside from copper, palladium is another widely studied active component for methanol reforming. When prepared on inert oxide supports, palladium is an effective decomposition catalyst, selectively forming hydrogen and carbon monoxide [5–8]. However, when palladium is prepared with ZnO or ZrO_2 the selectivity shifts to CO_2, for the SRM reaction. The change from carbon monoxide to carbon dioxide selectivity on palladium catalysts is attributed to the formation of Pd–Zn alloys, which have been shown to form under reduction conditions at moderate temperatures [9–11].

A number of researchers have reported positive effects from incorporating ZrO_2 in copper catalysts as a promoter

S. Schuyten · P. Dinka · A. S. Mukasyan · E. Wolf (✉)
Department of Chemical and Biomolecular Engineering, University of Notre Dame, Notre Dame, IN 46556, USA
e-mail: ewolf@nd.edu

or support. A CuO/ZrO_2 catalyst used in steam reforming was found to have higher activity than a commercial $CuO/ZnO/Al_2O_3$, while maintaining deactivation resistance [12]. Zirconia has also been shown to promote efficiency of $Cu/ZnO/Al_2O_3$ catalysts, producing hydrogen with low carbon monoxide levels [13–15]. Studies by Fisher and Bell that focused on the mechanism of methanol synthesis and decomposition demonstrated a synergy between copper and ZrO_2, where reaction intermediates were detected on the ZrO_2 phase [16–18].

Many techniques are used for complex oxide catalyst preparations, including, co-precipitation, sol–gel, solid-state, and mechano-synthesis methods [19–22]. In a previous work we studied the oxidative reforming of methanol in multicomponent catalysts [23]. Using a high throughput technique for catalyst activity evaluation we determined that a catalyst containing molar ratios of $7CuO/3ZnO/1ZrO_2$ with 1% Pd prepared by co-precipitation achieved 92% H_2 selectivity at 100% methanol conversion with only 1400 ppm of carbon monoxide produced. The co-precipitated catalysts had BET areas exceeding 60 m^2/g and were later (unpublished result) shown to be stable for at least 100 h on stream [23, 24]. The formulations using both copper and palladium active species was used as a basis in this work.

An attractive relatively new method to prepare complex oxides and advanced solid state materials is by combustion synthesis [25, 26]. The specific feature of this technique is that after local ignition, a self-sustaining reaction propagates throughout the mixture of precursors, leaving behind the desired product oxides. Originally, reactive mixtures were simply solid heterogeneous powders. Modification of this technique, so-called *solution combustion* synthesis, takes place in a liquid solution of the oxidizers (e.g. metal nitrites) and a fuel (e.g. glycine, citric acid, or urea). In the conventional scheme, called Volume Combustion Synthesis (VCS), the mixture is heated until auto-ignition occurs, leading to the formation of fine solid products with tailored composition.

Recently, we developed several novel modifications of solution combustion synthesis suitable for catalyst preparation [26, 27]. These methods include Self-Propagating Sol–gel Combustion (SSGC), Impregnated Support Combustion (ISC) and Impregnated Active Layers Combustion (ILC). The SSGC method involves room temperature drying of a metal nitrate and fuel solution to form a sol–gel like media that when locally ignited burns with a steady-state combustion front. For the ISC method, a reactive solution is impregnated into the porous structure of an inert high surface area support, with combustion occurring inside the pores of the heterogeneous media. The ISC method results in supported catalysts with high surface area, up to 200 $m^2\ g^{-1}$ [28]. For combustion mixtures that are endothermic or weakly exothermic the ILC method is useful because the reaction solution is impregnated into thin cellulose paper. Combustion of the cellulose paper provides additional energy to propagate the reaction.

The above methods require a localized ignition followed by steady-state combustion front propagation along the reactive media, allowing for a more controlled combustion compared to conventional VCS preparations. High temperature combustion accompanied by intensive gasification converts the precursors to a fine, highly crystalline powder. The reaction temperature can reach 1300 K, but reaction time, owing the rapid quenching of thin reacted layer, is on the order of 0.1–1 s, leading to catalysts with high surface area [27].

For this work three combustion based approaches were used to synthesize complex multifunctional catalysts containing oxides of copper, zinc, zirconium and palladium. These catalysts were tested for hydrogen activity from methanol partial oxidation and characterized by BET, N_2O decomposition, XRD, XPS, TPR, and SEM.

2 Experimental

2.1 Catalyst Synthesis

Mixtures of metal nitrates (Alfa Aesar) $Me^{\gamma}(NO_3)_{\gamma}$ -yH_2O (where Me = Cu, ZrO, Zn, or Pd) and glycine (as fuel) were used to synthesize catalysts in three combustion synthesis techniques: volume combustion synthesis (VCS), impregnated support combustion (ISC), and a novel combination of the VCS and ISC, so-called, second wave impregnation (SWI) approach.

More specifically, for the VCS method, reactants in desired concentrations were dissolved in water and stirred to reach homogenization. Under constant stirring the solution was slowly heated to evaporate water and concentrate reactants, until the self-ignition point T_{ig} of $\sim$525 K was reached. After ignition, the temperature rose rapidly, $\sim 10^3$ K s^{-1} to values up to 1300 K. In general, under equilibrium conditions, the combustion reaction in such systems can be represented as in Eq. 1:

$$\begin{aligned} \mathrm{Me(NO_3)}_v + \left(\frac{5}{9}v\phi\right)\mathrm{C_2H_5NO_2} + \left[v\frac{5}{4}(\phi - 1)\right]\mathrm{O_2} \\ \rightarrow \mathrm{MeO}_{v/2} + \left(\frac{10}{9}v\phi\right)\mathrm{CO_2} + \left(\frac{25}{18}\phi v\right)\mathrm{H_2O} \\ + \left[\frac{v(5\phi + 9)}{18}\right]\mathrm{N_2} \end{aligned} \quad (1)$$

where Me—is a metal with valence v, ϕ is a fuel to oxidizer ratio. With $\phi = 1$ the fuel and oxidizer are added in stoichiometric amounts and atmospheric oxygen is not needed for complete oxidation of the fuel. The values $\phi > 1$or $\phi < 1$ implies fuel rich or lean conditions, respectively. For example, a synthesis of a CuO/ZnO

catalyst has the reaction stoichiometry found in Eq. 2, with $\phi = 1$:

$$Cu(NO_3)_2 + Zn(NO_3)_2 + \frac{20}{9}C_2H_5NO_2 \rightarrow CuO + ZnO + \frac{40}{9}CO_2 + \frac{50}{9}H_2O + \frac{28}{9}N_2 \quad (2)$$

In previous works [29, 30] we have used two approaches for noble metal incorporation into oxide-based materials: "internal"; during volume solution combustion synthesis, and "external"; metal co-precipitation after VCS. It was shown that in the former case, where the catalyst was synthesized by adding a metal containing precursor (e.g. tetra-ammine-platinum nitrate) into the initial metal nitrate and glycine solution, leads to higher catalytic activity. In this work, a novel approach was used to load palladium onto the catalyst in addition to the internal VCS method, i.e. SWI method. During this procedure, a VCS synthesized complex oxide catalyst powder was immersed into a reaction solution containing the Pd-based nitrate precursor and fuel. A second combustion reaction leads to the metal incorporation onto the complex oxide support.

Catalysts synthesized by the ISC method utilized ZrO_2 and Al_2O_3 (Alfa Aesar) supports with high surface areas, 125 and 149 $m^2\ g^{-1}$ respectively. The pellets of oxide supports were sieved and impregnated by combustion reaction solutions of desired compositions, followed by ignition with a heated tungsten wire.

Catalysts are named according to their prepared compositions and are listed in Table 1. The metals CuO, ZnO, ZrO_2 are given in respective molar ratios, with Pd as weight percent based on the total oxide mass, followed by the synthesis mode VCS, ISC, or SWI, and finally the fuel/oxidizer ratio ϕ, or the support material. For example, catalyst 7Cu/3Zn/1Zr/3Pd-VCS-0.5 corresponds to a 7CuO:3ZnO:1ZrO_2 molar ratio, with 3 wt.% palladium prepared by the VCS method with a fuel/oxidizer ratio of 0.5. All ISC and SWI catalysts were prepared with $\phi = 0.5$.

2.2 Catalytic Activity

Activity measurements were conducted in a quartz tubular reactor with an internal diameter of 10.5 mm and total length 30 cm. For each experiment, fresh catalyst powder was pressed at 35 MPa for 4 min. The resulting pellet was broken and sieved to obtain a particle size between 0.6 and 1 mm. A mass of 200 mg sieved catalyst was used in each experiment, supported by quartz wool inside the reactor tube. Each catalyst was reduced *in situ* by heating from room temperature at a rate of 5 K min^{-1} to 573 K and held for one hour under a pure hydrogen flow rate of 50 cc min^{-1}. After reduction, the flow was switched from hydrogen to nitrogen as the reactor was cooled to room temperature over the course of about 30 min. Reactant flow rate was 140 cc min^{-1} of nitrogen saturated with methanol at 0 °C, resulting in a stream containing 3.8% methanol. Oxygen was added to the reactant stream at a rate of 2.8 cc min^{-1}, yielding an O_2/CH_3OH ratio of 0.5. An overall pressure less than 3.0 kPa was carefully maintained inside the reactor to provide constant pressure in the GC sampling system.

Two gas chromatographs were connected in parallel to analyze reactor effluent. The first, Varian 3300, contained a 3.7 m HAYESEP Q column for separation and detection of carbon dioxide, methanol, water, and formaldehyde. The second, Varian 920, contained a 1.8 m molecular sieve 5A and a 5.0 m HAYESEP D connected in series capable of separating nitrogen, oxygen, hydrogen, carbon monoxide, and methane. Product gases were measured in 12 min intervals while the catalyst bed was heated from room temperature to 573 K over the course of 3 h.

Table 1 BET surface area and carbon content for catalysts prepared by VCS

Catalyst	BET area ($m^2\ g^{-1}$)	Carbon content (wt. %)
7Cu/3Zn/1Zr/3Pd-VCS-0.5	14	0.28
7Cu/3Zn/1Zr/0Pd-VCS-0.5	18	0.19
6Cu/2Zn/3Zr/3Pd-VCS-0.5	14	0.32
6Cu/2Zn/3Zr/3Pd-VCS-3.0	4.9	5.7

2.3 Characterization Methods

Mean and specific copper surface areas were measured by the well-known nitrous oxide decomposition method [31–35] where nitrous oxide reacts with surface Cu^0 with the following stoichiometry:

$$2Cu + N_2O \rightarrow Cu_2O + N_2 \quad (3)$$

To minimize oxidation of subsurface copper layers a pulse method was used. Each pulse has a short contact time, 1–2 s, and a low reactant concentration with the reactor at 333 K. At least 100 mg of fresh sieved catalyst was loaded into a quartz reactor setup identical to the one used in activity experiments. The sample was reduced by flowing 5% hydrogen in argon, heating to temperature of 573 K, the flow was then switched to nitrogen while the temperature was maintained for 10 min to clean any residual hydrogen or water. Following reduction, the temperature of the reactor was quickly reduced to 333 K, which was maintained constant for the duration of the experiment. Pulses of 1 cm^3 5% nitrous oxide in nitrogen were injected into the carrier stream of nitrogen flowing at 50 $cm^3\ min^{-1}$ until complete oxidation of the Cu^0 surface

to Cu^{+1} occurred. Uptake of N_2O was monitored with a gold plated tungsten filament TCD at a current of 90 mA. Dispersion, mean, and specific surface areas were calculated assuming a copper surface atomic density of $1.47*10^{19}$ atoms-m^{-2}. No nitrous oxide reaction or adsorption could be attributed to palladium, when attempted in the absence of copper on various supports.

BET surface area was measured with a Quantachrom Corporation Monosorb unit that utilizes a dynamic technique with a TCD. A mixture of 30% nitrogen and 70% helium was used as both carrier and adsorbent gas. Catalysts analyzed in the BET had a particle size sieved between 0.6 and 1.0 mm. The resulting particles were precisely weighed and out-gassed for 30 min at a temperature of 523 K. No other pretreatment procedures were carried out prior to BET measurement.

Temperature programmed reduction (TPR) experiments were conducted to determine copper reducibility in the catalysts. 75 mg of fresh sieved catalyst was loaded into a quartz reactor in a setup identical to the activity experiments described above. The experiments started at room temperature with flowing 5% hydrogen in argon at 100 cm^3 min^{-1}, and a heating rate of 5 K min^{-1} up to 620 K, ensuring complete reduction of CuO to Cu^0. Hydrogen uptake was measured using a TCD with a gold plated tungsten filament at a current of 90 mA and a detector temperature of 318 K. Water was removed from the reactor effluent prior to the TCD by passing through a small stainless steel coil immersed in a bath of acetone, 2-propanol, and dry ice.

Freshly calcined untreated catalyst powders were analyzed via X-ray diffraction (XRD) and X-ray photoelectron spectroscopy (XPS). XRD patterns were collected in a Scintag Inc. X-1 diffractometer with a Cu–Kα source operating at 30 kV and 30 mA and X-ray wavelength of 0.154056 nm. Scanning parameters for all samples were 2θ scans from 25 to 80 degrees with a step size of 0.02 degrees and a 3 s dwell time.

XPS measurements were conducted on a Kratos XSAM 800 spectrometer with a monochromatic Al–Kα X-ray source operating at 1486.6 eV and a takeoff angle fixed at 90 degrees. The powder samples of fresh unreduced catalyst were adhered to sample mounts using a conductive carbon tape. XPS analysis was performed with vacuum chamber with pressure less than 2×10^{-8} torr. Raw data was processed with CasaXPS software package, with relative sensitivity factors obtained from the Kratos XSAM library.

Powder microstructure of ISC prepared ZrO_2 supported catalysts was studied by field emission scanning electron microscopy (SEM) on an LEO series EVO 50 microscope equipped with Energy-Dispersive System (EDS). Samples were prepared by encasing catalyst pellets ranging in size from 0.6 to 1.0 mm in epoxy resin. Upon drying, the surface was polished to obtain cross sections of the embedded pellets normal to the polished surface. To enhance electrical conductivity, a layer of gold approximately 2 nm thick was sputtered onto the surface of the sample.

Finally, the overall quantities of main elements in catalysts were obtained by ICP-MS analysis (Univ. Illinois, Urbana, IL), while small amounts of carbon and sulfur contents were measured by elemental combustion analysis on a Costech Analytical Technologies Inc., model 4010.

3 Results and Discussion

3.1 Volume Combustion Synthesis Catalysts

Catalytic activity expressed as conversion vs. temperature for catalysts prepared via VCS are presented in Fig. 1. The effects of fuel/oxidizer ratio ϕ and addition of palladium as a catalyst promoter are compared. For palladium containing catalysts 6Cu/2Zn/3Zr/3Pd-VCS-ϕ, the value of ϕ was varied from a lean fuel $\phi = 0.5$ preparation in 6Cu/2Zn/3Zr/3Pd-VCS-0.5 to the fuel rich $\phi = 3.0$ preparation 6Cu/2Zn/3Zr/3Pd-VCS-3. The lean fuel preparation ($\phi = 0.5$) shows significantly higher methanol conversion at all temperatures than the fuel rich preparation. A catalyst synthesized with $\phi = 1$ (not depicted) has intermediate behavior.

The difference in activity between the 6Cu/2Zn/3Zr/3Pd-VCS-0.5 and the 6Cu/2Zn/3Zr/3Pd-VCS-3.0 catalysts can be attributed to morphological differences. Table 1 contains the carbon content and BET area of catalysts shown in Fig. 1. The $\phi = 0.5$ catalysts have a greater BET surface area, 14 m^2 g^{-1}, nearly 3 times larger than the

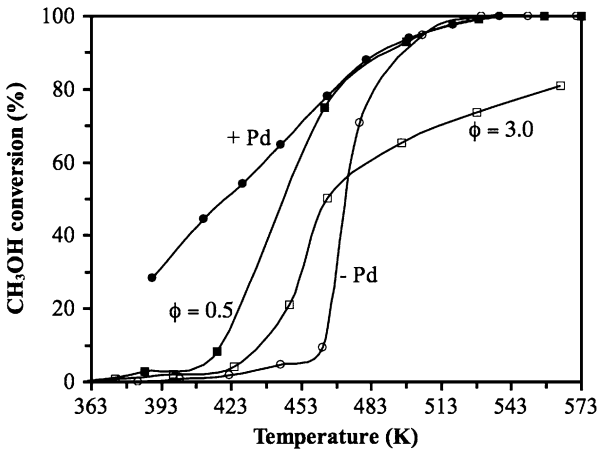

Fig. 1 Catalytic activity as methanol conversion vs. temperature for catalysts prepared via VCS. (◯) 7Cu/3Zn/1Zr/0Pd-VCS-0.5 (−Pd), (●) 7Cu/3Zn/1Zr/3Pd-VCS-0.5 (+Pd), (■) 6Cu/2Zn/3Zr/3Pd-VCS-0.5, (□) 6Cu/2Zn/3Zr/3Pd-VCS-3.0

$\phi = 3.0$ catalyst at 4.9 m^2/g. Moreover, approximately 6 wt.% of the $\phi = 3.0$ is carbon, while only 0.3 wt.% of the $\phi = 0.5$ catalysts was found to be carbon.

For a fuel rich synthesis mixture combustion temperatures are higher than in a lean mixture due to additional reaction between the glycine fuel and atmospheric oxygen. The higher temperatures result in a catalyst with larger crystallites and lower surface area from particle sintering. XRD patterns in Fig. 2 clearly show broader diffraction lines for 6Cu/2Zn/3Zr/3Pd-VCS-0.5, qualitatively indicative of smaller crystallites compared to 6Cu/2Zn/3Zr/3Pd-VCS-3.0. CuO crystallite size estimated by the Scherrer equation in the $\phi = 0.5$ catalysts was 7 nm, compared to 14 nm in the $\phi = 3.0$ catalyst.

The XRD patterns in Fig. 2 also reveal differences in the ZrO_2 phases present in the fresh catalyst. The pattern for the 6Cu/2Zn/3Zr/3Pd-VCS-0.5 sample shows a broad asymmetric peak at $2\theta = 30.5°$, which is taken to be overlapping tetragonal ZrO_2 and hexagonal ZnO peaks at $2\theta = 30.3°$ and 31.7°, respectively. Catalyst 6Cu/2Zn/3Zr/3Pd-VCS-3.0 has sharp defined peaks for both tetragonal ZrO_2 and ZnO in the same 2θ region. A separate peak which is not present in the 6Cu/2Zn/3Zr/3Pd-VCS-3.0 catalyst is attributed to monoclinic ZrO_2 at $2\theta = 30.3°$. Only monoclinic ZrO_2 is thermodynamically stable at room temperature [36], however the tetragonal transition temperature may be lowered by incorporating certain materials with ZrO_2 [37].

The increased carbon content present in fuel rich preparations ($\phi > 1$) is likely due to oxygen diffusion limitations resulting in incomplete combustion of the glycine fuel. Carbon found in combustion-synthesized catalysts is not due to carbon buildup normally associated with hydrocarbon reactions, which occurs primarily on the surface of active catalysts. Presumably, the carbon found in the 6Cu/2Zn/3Zr/3Pd-VCS-3.0 catalyst is distributed throughout the bulk as a synthesis byproduct. Carbon may lower surface area by filling voids and pores, especially where rapid oxygen transport from air is necessary for complete combustion as in fuel-rich conditions, and/or blocking of surface reaction sites, leading to lower activity [38]. In addition, the dispersed carbon may also hinder spillover between components on the surface of the catalyst. Similarly, interactions between the active copper and palladium components and the oxides of zinc and zirconium, such as alloy formation, stabilization of the active phase, and structure-activity effects may be weaker because of carbon blocking phase interactions. Thus it can be concluded that several mechanisms are involved in altering the structure of a fresh catalysts due to changing the fuel/oxidizer ratio.

Figure 1 also demonstrates the influence of catalyst bulk composition on activity. The 7Cu/3Zn/1Zr/3Pd-VCS-0.5 catalyst, which contains 45 wt.% copper and 3 wt.% palladium is significantly more active than the 7Cu/3Zn/1Zr/0Pd-VCS-0.5 catalyst without palladium. The 6Cu/2Zn/3Zr/3Pd-VCS-0.5 catalyst contains 37 wt.% copper and 3 wt.% palladium has slightly lower activity at temperatures below 460 K. Surface areas, carbon content, and particle size measured for these two catalysts were nearly identical, indicating that another factor, such as copper dispersion could be determining catalytic activity. These results agree with our previous observations where a co-precipitated catalyst having a composition of 45 wt.% copper promoted with both palladium and zirconia was shown to be the optimum composition [23].

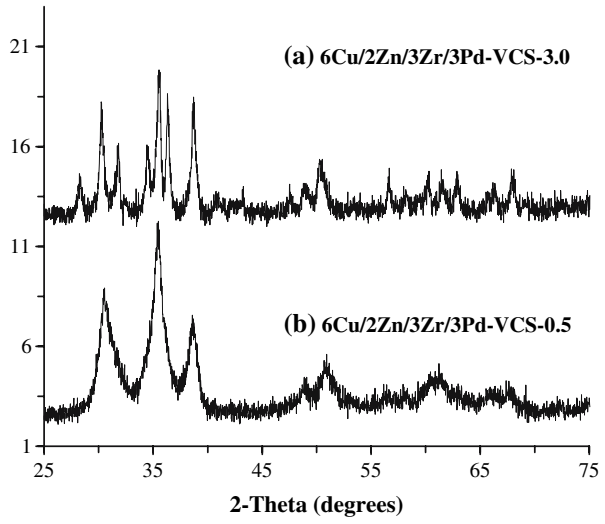

Fig. 2 XRD patterns of fresh catalysts prepared by VCS, (**a**) 6Cu/2Zn/3Zr/3Pd-VCS-3.0 with $\phi = 3$ and (**b**) 6Cu/2Zn/3Zr/3Pd-VCS-0.5 with $\phi = 0.5$

3.2 Impregnated Support Combustion Catalysts

The activity curves of two ISC preparations supported on Al_2O_3 and ZrO_2 are shown in Fig. 3. The active oxide phases were loaded on two different supports, γ-Al_2O_3 and monoclinic ZrO_2. Comparison of 7Cu/3Zn/1Zr/1Pd-ISC-Al and 7Cu/3Zn/1Zr/3Pd-ISC-Zr shows that the ZrO_2 supported catalyst exhibits significantly higher methanol conversion activity at nearly all temperatures compared to the γ-Al_2O_3 supported catalyst.

As expected, both catalysts prepared by ISC have high BET areas from the support and thus are several times higher then any of the bulk catalysts in this study. In Table 2, the BET surface area of the 7Cu/3Zn/1Zr/1Pd-ISC-Al on $\tilde{\gamma}$-Al_2O_3 is 170 m^2 g^{-1}, is greater than the 149 m^2 g^{-1} of the initial support. Conversely, the area of the catalyst prepared on ZrO_2 is 82 m^2 g^{-1}, lower than the 125 m^2 g^{-1} of the support. The total BET surface area does

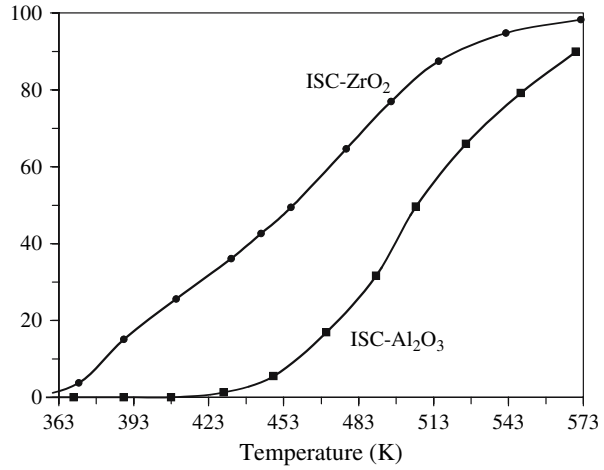

Fig. 3 Catalytic activity as methanol conversion vs. temperature for catalysts prepared via ISC; (●) 7Cu/3Zn/1Zr/3Pd-ISC-ZrO_2 and (◯) 7Cu/3Zn/1Zr/1Pd-ISC-Al_2O_3

not correlate with catalyst activity in this case, since the area difference is nearly a factor of two, compared with the VCS prepared catalysts which have similar activity, but much lower area.

The difference in activity may be partially explained from N_2O decomposition data also found in Table 2. The copper surface area measured for the 7Cu/3Zn/1Zr/3Pd-ISC-Zr catalyst was 2.2 $m^2\ g^{-1}$, while for the 7Cu/3Zn/1Zr/1Pd-ISC-Al catalyst Cu^0 area was less than 1 $m^2\ g^{-1}$. This result agrees with other studies that have shown copper surface area correlates with activity better than total BET area.

The thickness of the combustion impregnated layer on the ZrO_2 supported catalyst was determined by SEM and EDS. Figure 4 is an SEM backscattering image of a cross section of a typical 7Cu/3Zn/1Zr/3Pd-ISC-Zr catalyst particle. EDS analysis of the various points identified in Fig. 4 and listed in Table 3, show that the thickness of the active layer is on the order of 20 μm, which is similar to those reported for Fe_2O_3 supported on Al_2O_3 [28]. The concentration of copper decreases from 80:10 as Cu:Zr weight ratio near the surface to 10:90 at a depth of $\sim$20 μm.

X-ray diffraction for the 7Cu/3Zn/1Zr/3Pd-ISC-Zr catalyst post reduction in hydrogen (not shown) has no peaks corresponding to palladium or zinc, due to overlap of the support peaks and the small amount of these components in the sample. The main peak attributable to the combusted layer was located at $2\theta = 43.2$ degrees corresponding to $\langle 111 \rangle$ Cu^0, support peaks overlap the rest. Application of the Scherrer equation to the Cu $\langle 111 \rangle$ peak gives an estimate of the reduced copper particle size of 14 nm. The support oxide phase was not modified by the combustion synthesis reaction since only monoclinic ZrO_2 was detected by XRD.

Table 2 Total BET and copper surface areas for catalysts prepared by the ISC method

Catalyst	BET area ($m^2\ g^{-1}$)	Cu area N_2O ($m^2\ g^{-1}$)
7Cu/3Zn/1Zr/1Pd-ISC-Al	170	<1.0
7Cu/3Zn/1Zr/3Pd-ISC-Zr	82	2.2

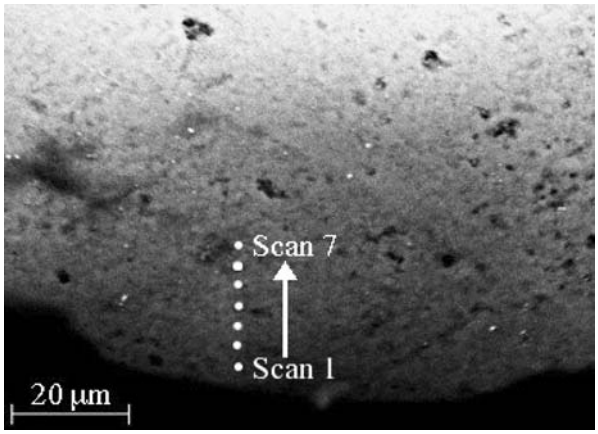

Fig. 4 EDX line scan of a ISC loaded ZrO_2 particle cross section for catalyst 7Cu/3Zn/1Zr/3Pd-ISC-Zr

Table 3 EDX line analysis of copper and zirconium elements as weight ratio vs. depth, corresponding to SEM image of a cross section of catalyst 7Cu/3Zn/1Zr/3Pd-ISC-Zr in Fig. 4

EDX point spectrum	Depth (μm)	Cu weight ratio	Zr weight ratio
1	2.5	79	11
2	5.6	63	26
3	9.2	47	45
4	12	23	69
5	15	11	81
6	19	9	81
7	22	7	87

3.3 Second Wave Impregnation Combustion Catalysts

Figure 5 is a comparison of conversion vs. temperature on catalysts in which palladium was loaded by VCS and SWI methods, all with $\phi = 0.5$. The catalysts with palladium prepared by VCS, 7Cu/3Zn/1Zr/3Pd-VCS-0.5 and 7Cu/3Zn/0Zr/3Pd-VCS-0.5, with and without ZrO_2 respectively, show slightly lower activity for POM compared to SWI preparations, where the palladium is concentrated on the surface. Figure 5 also shows that the catalysts containing ZrO_2 are slightly more active than those without it. The ZrO_2 promoted catalyst reaches 90% conversion at

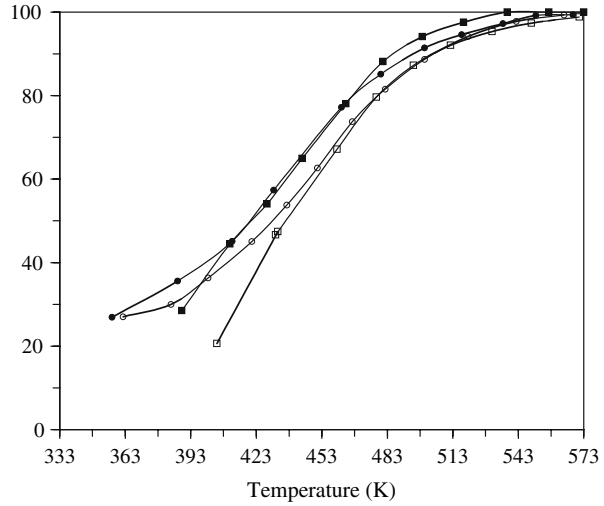

Fig. 5 Catalytic activity as methanol conversion vs. temperature for catalysts prepared via VCS and SWI; (◯) 7Cu/3Zn/0Zr/3Pd-SWI-0.5, (●) 7Cu/3Zn/1Zr/3Pd-SWI-0.5, (■) 7Cu/3Zn/1Zr/3Pd-VCS-0.5, (□) 7Cu/3Zn/0Zr/3Pd-VCS-0.5

483 K, compared with the catalyst without ZrO_2 reaching the same conversion at 488 K.

Catalyst compositions for two selected catalysts with different palladium loading methods verified via ICP-MS are presented in Table 4. The compositions obtained were similar to the target values for all observed components. For example, the copper content in 7Cu/3Zn/0Zr/3Pd-SWI-0.5 was measured to be 53.6 wt.% copper, while the preparative target value was 54.3 wt.%. Palladium loadings were also close to target compositions, with less than 5% error.

The Cu/Pd ratio on the surface of catalysts prepared via VCS and SWI techniques was determined using XPS. Concentration and shift of the Pd 3d peak could not be observed in catalysts containing ZrO_2 because of overlap with the intense Zr 3p peak. Therefore only catalysts 7Cu/3Zn/0Zr/3Pd-VCS-0.5 and 7Cu/3Zn/0Zr/3Pd-SWI-0.5, without Zr, were compared. These catalysts were analyzed via XPS as synthesized, and surface compositions of working catalysts are likely different due to reduction or reaction. The palladium 3d doublet corresponding to PdO at 337 eV and 343 eV was easily detected for both 7Cu/3Zn/0Zr/3Pd-SWI-0.5 and 7Cu/3Zn/0Zr/3Pd-VCS-0.5 catalysts. Table 5 lists quantified Cu/Pd surface ratios for these catalysts. The amount of palladium quantified on the surface is significantly greater for the 2-step impregnation than for conventional VCS sample, which is expected. Indeed, the surface Cu/Pd ratio goes from ~70 to 4, a 17 fold increase in the relative amount of surface palladium. This result further demonstrates the viability of the SWI method as a method for loading active phases onto catalyst supports. It should be noted that Pd alone does not catalyze POM. A reference catalyst prepared with Pd on an inert support such as SiO_2 produced formaldehyde, and combustion and decomposition products depending on the reactor temperature.

Table 5 BET, N_2O total, mean Cu surface area (MSA), and the Cu/Pd ratio observed in XPS for VCS and SWI catalysts

Catalyst	BET area ($m^2\ g^{-1}$)	Total Cu area ($m^2\ g^{-1}$)	N_2O Cu MSA ($m^2\ gCu^{-1}$)	XPS Cu/Pd ratio
7Cu/3Zn/0Zr/3Pd-VCS-0.5	9.0	3.2	5.0	67
7Cu/3Zn/0Zr/3Pd-SWI-0.5	18	4.7	8.6	3.9
7Cu/3Zn/1Zr/3Pd-VCS-0.5	11	12	22	N/A
7Cu/3Zn/1Zr/3Pd-SWI-0.5	19	14	25	N/A

Powder X-ray diffraction patterns obtained for catalysts 7Cu/3Zn/0Zr/3Pd-SWI-0.5 and 7Cu/3Zn/0Zr/3Pd-VCS-0.5 are presented in Fig. 6. The only measurable peaks are those of BCC CuO and hexagonal ZnO phases. No peaks directly attributable to palladium were detected due to relatively small amounts of this metal as well as overlapping of peaks. The XRD lines for the SWI catalyst are noticeably sharper in contrast to the VCS sample. A calculation using the Scherrer equation yields crystalline size of 7 nm for VCS CuO and 13 nm for SWI sample. The difference in crystalline size is likely due to exposure of the catalyst to the second high temperature combustion reaction, causing particle sintering. Additionally, during the SWI synthesis, the fuel itself may reduce the oxide phases present in the support, accelerating the sintering process.

BET and copper surface areas for the SWI catalysts 7Cu/3Zn/0Zr/3Pd-SWI-0.5 and 7Cu/3Zn/0Zr/3Pd-SWI-0.5 are presented in Table 5. These results show that while promotion with ZrO_2 has only a small influence on the BET area, SWI catalysts show an increase in total surface area from roughly 10 $m^2\ g^{-1}$ to 18 $m^2\ g^{-1}$ compared to VCS catalysts of the same composition. Also, Cu^0 area is

Table 4 Comparison of observed ICP-MS and target compositions for a SWI and a VCS prepared catalyst

Catalyst	Cu wt.%		Zn wt.%		Pd wt.%	
	Target	ICP-MS	Target	ICP-MS	Target	ICP-MS
7Cu/3Zn/0Zr/3Pd-VCS-0.5	53.6	49.3	23.7	22.6	3.0	2.9
7Cu/3Zn/0Zr/3Pd-SWI-0.5	53.6	54.3	–	–	3.0	3.0

increased by nearly a factor of 3 upon promotion with ZrO_2. SWI preparations also show a small increase in copper area. The copper area found to be slightly larger than the BET area for catalyst 7Cu/3Zn/1Zr/3Pd-VCS-0.5 may be due to structural changes which occur on reduction, including a loss of ~10% total mass from oxygen or from oxidation of subsurface copper layers.

Other groups have observed increases in copper dispersion upon promotion with ZrO_2 due to increased sintering resistance [39]. The dispersion increase is normally accompanied by an increase in BET area and a decrease in particle size. In this case, copper particle size was only influenced by the preparation, not by the promotion with ZrO_2. This effect can also be seen by comparing XRD patterns in Fig. 2 with Fig. 6, where both unpromoted and zirconia promoted catalysts have an identical CuO particle size of 7 nm. Both large copper particles in the SWI preparations and small particles in the VCS preparation show an increase in copper dispersion, indicating that the ZrO_2 does not increase sintering resistance during combustion synthesis preparation.

TPR profiles coresponding to the reduction of CuO for selected combustion synthesized catalysts are shown in Fig. 7 in units equivalent to hydrogen uptake rate vs. temperature. No peaks could be attrubuted to the reduction of PdO or decomposition of Pd hydride in the temperature ranges investigated. Unpromoted CuO/ZnO or 7Cu/3Zn/0Zr/0Pd-VCS-0.5 catalyst has the highest reduction temperature of the catalysts studied. The reduction initiates at ~500 K, beginning in a loosely Gaussian distribution through to the maximum H_2 uptake peaks at 529 K. Then a small apparent overlapping peak contributes to a tail which extends to the completion of reduction at ~573 K. The higher temperature of this reduction peak is another indication of relatively large CuO crystallites with a wide size distribution, consistent with observed XRD results.

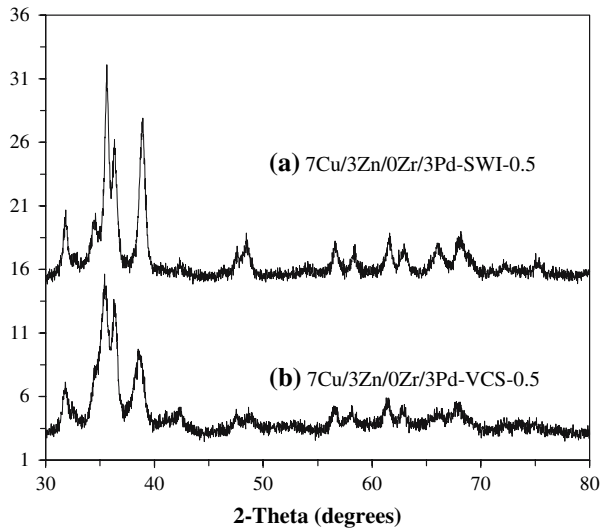

Fig. 6 XRD patterns of catalysts with composition prepared by SWI and VCS methods (**a**) 7Cu/3Zn/0Zr/3Pd-SWI-0.5, (**b**) 7Cu/3Zn/0Zr/3Pd-VCS-0.5

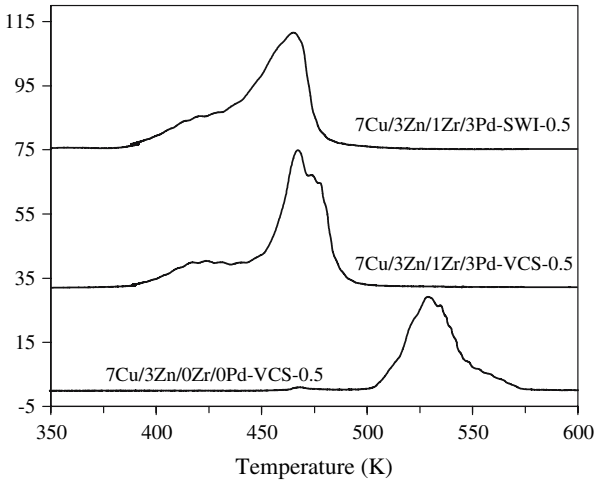

Fig. 7 Hydrogen TPR profiles for catalysts 7Cu/3Zn/0Zr/0Pd-VCS-0.5 (bottom), 7Cu/3Zn/1Zr/3Pd-VCS-0.5 (middle), and 7Cu/3Zn/1Zr/3Pd-SWI-0.5 (top)

Catalysts promoted with palladium show a significant decrease in reduction temperature compared to the standard CuO/ZnO catalyst. Both 7Cu/3Zn/1Zr/3Pd-VCS-0.5 and 7Cu/3Zn/1Zr/3Pd-SWI-0.5 have hydrogen uptake maximums near 385 K with reduction ending at approximately 500 K. These reduction profiles indicate a complex reduction behavior, which is influenced by the palladium loading method. The SWI catalyst exhibits a larger very broad initial uptake peak and lack of a post peak shoulder. This result is consistent with other studies, which have shown that addition of palladium to CuO systems modifies the reduction of copper [40, 41]. This effect has been attributed to spillover of dissociated hydrogen from palladium to copper species [40]. Therefore the higher surface concentration of palladium in the SWI catalyst, as verified by XPS, may reduce surface copper at lower temperature, while the loss of the post peak shoulder could be a result of greater contact between surface palladium and gas phase hydrogen.

3.4 Catalyst Selectivity

Hydrogen, carbon dioxide, and carbon monoxide selectivities at 453 K and the temperature of maximum hydrogen selectivity for combustion synthesized catalysts are presented in Table 6. The most active catalysts have high conversions and selectivities at 453 K. Any carbon monoxide produced remained below the GC detection limit of

Table 6 Conversion and selectivity data for selected catalysts

Catalyst	Statistics at 453 K				Statistics at maximum H_2 selectivity			
–	CH_3OH % conversion	H_2 % selectivity	CO_2 % selectivity	Temp K	CH_3OH % conversion	H_2 % selectivity	CO_2 % selectivity	CO ppm
7Cu/3Zn/0Zr/0Pd-VCS-0.5	10	0.0	14	528	95	96	98	1000
7Cu/3Zn/0Zr/3Pd-VCS-0.5	62	56	88	512	92	94	93	2000
7Cu/3Zn/1Zr/3Pd-VCS-0.5	72	72	89	499	94	97	94	1700
7Cu/3Zn/1Zr/0Pd-VCS-0.5	7	0	26	505	95	95	99	800
6Cu/2Zn/3Zr/3Pd-VCS-3.0	30	11	93	528	74	67	83	3500
7Cu/3Zn/1Zr/1Pd-ISC-Al	6	0	99	548	79	70	80	4800
7Cu/3Zn/1Zr/3Pd-ISC-Zr	49	31	81	515	87	85	92	2100
7Cu/3Zn/0Zr/3Pd-SWI-0.5	63	58	90	520	94	94	94	2600
7Cu/3Zn/1Zr/3Pd-SWI-0.5	72	73	90	500	91	96	96	1000

Selectivity data is listed for all catalysts at 453 K and at the temperature where maximum hydrogen selectivity was reached

500 ppm at this temperature. Generally hydrogen selectivity achieved similar levels at conversions >50% and temperatures <525 K. At very low methanol conversions, the complete methanol combustion reaction dominates, producing mostly water and carbon dioxide. In the absence of oxygen, combustion synthesis preparations catalyze the methanol decomposition reaction. Under partial oxidation conditions at temperatures above 523K, both H2O and CO byproducts increase with temperature, indicating that RWGS activity and methanol decomposition are likely occurring

A small amount of formaldehyde was also detected at low conversions, especially in catalysts containing palladium. At temperatures >523 K increasing amounts of carbon monoxide is produced either as part of the reverse water gas shift reaction and/or as a product of methanol decomposition, with the former occurring over more active catalysts and the latter over less active. The highest carbon dioxide and hydrogen selectivity achieved with the catalyst is also presented in the table along with the conversion and temperature it took place. While most of the catalysts achieved relatively high conversion and selectivity at elevated temperatures, it also resulted in greater CO byproduct formation.

It should be noted that the catalysts with the highest hydrogen selectivity contained no palladium, however this slight increase in hydrogen yield requires significantly higher reaction temperatures, which are less desirable to operate at due to increased carbon monoxide byproduct formation and reduced catalytic lifetime. The decrease in hydrogen production in the palladium free catalysts could also be due to reactor hotspots and changes in the oxidation state of copper. Generally the maximum selectivity for both hydrogen and carbon dioxide were greater than 90% for all active catalysts.

4 Conclusions

Active and selective catalysts for the partial oxidation of methanol were prepared by novel combustion synthesis techniques including volume combustion synthesis, impregnated support combustion, and second wave impregnation.

Catalysts prepared by conventional VCS techniques were found to be highly sensitive to the fuel/oxidizer ratio in preparation. Materials synthesized with a fuel rich $\phi > 1$ mixture had lower catalyst surface area and activity, with high carbon content and larger crystallite size. The fresh fuel rich preparations also contained monoclinic ZrO_2 while the lean preparation contained only dispersed tetragonal ZrO_2. Adding palladium to the catalyst significantly enhanced overall catalytic activity, with similar activity compared to our previous study [23].

The catalyst prepared by the SWI method, 7Cu/3Zn/1Zr/3Pd-SWI-0.5, had similar activity compared to the 7Cu/3Zn/1Zr/3Pd-VCS-0.5 preparation, despite the increased dispersion of palladium on the surface. Including zirconia in the preparation had a greater effect on activity than the palladium loading method but little effect on physical characteristics, while palladium loading method did not significantly influence activity, but did have an effect on CuO particle size, BET, and copper surface area.

This work represents a first look at supported ISC and SWI preparations, which showed high activity and selectivity for the partial oxidation of methanol. Methanol conversion reached 90% at 510 K for the ZrO_2 supported and 570 K for the Al_2O_3 supported ISC catalysts catalyst. The active supported layer was found to be approximately 20 μm deep in the ZrO_2 support. Subjecting SWI synthesized materials to an additional combustion impregnation results in concentrating the active layer on the surface of

the catalyst at a cost of larger particle size. Further work is ongoing in our laboratory to produce an improved second generation of combustion synthesized catalysts for methanol reforming.

Acknowledgment SS and EEW gratefully acknowledge funding from the International Copper Association (ICA) for support of this work. AM and PD were supported by the U.S. Army CECOM RDEC through Agreement DAAB07-03-3-K414. Such support does not constitute endorsement by the U.S. Army of the views expressed in this publication.

References

1. Demirbas AF (2004) Energy Explor Exploit 22:231–239
2. Farrauto R, Hwang S, Shore L, Ruettinger W, Lampert J, Giroux T, Liu Y, Ilinich O (2003) Ann Rev Mater Res 33:1–27
3. Trimm DL, Onsan ZI (2001) Catal Rev Sci Eng 43:31–84
4. Brown LF (2001) Int J Hydrogen Energy 26:381–397
5. Usami Y, Kangawa K, Kawazoe M, Matsumura Y, Sakurai H, Haruta M (1998) Appl Catal A Gen 171:123–130
6. Kapoor MP, Ichihashi Y, Kuraoka K, Shen WJ, Matsumura Y (2003) Catal Lett 88:83–87
7. Kapoor MP, Ichihashi Y, Kuroka K, Matsumura Y (2003) J Mol Catal A Chem 198:303–308
8. Lenarda M, Moretti E, Storaro L, Patrono P, Pinzari F, Rodriguez-Castellon E, Jimenez-Lopez A, Busca G, Finocchio E, Montanari T, Frattini R (2006) Appl Catal A Gen 312:220–228
9. Cubeiro ML, Fierro JLG (1998) Appl Catal A Gen 168:307–322
10. Cubeiro ML, Fierro JLG (1998) J Catal 179:150–162
11. Iwasa N, Takezawa N (2003) Top Catal 22:215–224
12. Purnama H, Girgsdies F, Ressler T, Schattka JH, Caruso RA, Schomacker R, Schlogl R (2004) Catal Lett 94:61–68
13. Velu S, Suzuki K, Kapoor MP, Ohashi F, Osaki T (2001) Appl Catal A Gen 213:47–63
14. Velu S, Suzuki K, Okazaki M, Kapoor MP, Osaki T, Ohashi F (2000) J Catal 194:373–384
15. Velu S, Suzuki K, Osaki T (1999) Chem Commun 2341–2342
16. Fisher IA, Bell AT (1999) J Catal 184:357–376
17. Fisher IA, Bell AT (1998) J Catal 178:153–173
18. Fisher IA, Bell AT (1997) J Catal 172:222–237
19. Xi JY, Wang ZF, Lu GX (2002) Appl Catal A Gen 225:77–86
20. Yuh J, Nino JC, Sigmund WA (2005) Mater Lett 59:3645–3647
21. Shi M, Liu N, Xu YD, Wang C, Yuan YR, Majewski P, Aldinger F (2005) J Mater Process Technol 169:179–183
22. Zyryanov VV, Sadykov VA, Uvarov NF, Alikina GM, Lukashevich AI, Neophytides S, Criado JM (2005) Solid State Ionics 176:2813–2818
23. Schuyten S, Wolf EE (2006) Catal Lett 106:7–14
24. Wolf EE, Schuyten SJ, Suh DJ (2007) In: Potyrailo RA, Maier WF (eds) Combinatorial and high-throughput discovery and optimization of catalysts and materials, ch 7, CRC press
25. Patil KC, Aruna ST, Mimani T (2002) Curr Opin Solid State Mater Sci 6:507–512
26. Mukasyan AS, Epstein P, Dinka P (2007) Proc Combust Inst 31(2):1789–1795
27. Mukasyan AS, Dinka P (2007) Adv Eng Mater 9:653–657
28. Dinka P, Mukasyan AS (2005) J Phys Chem B 109:21627–21633
29. Deshpande K, Mukasyan A, Varma A (2006) J Power Sources 158:60–68
30. Lan A, Mukasyan A (2007) J Phys Chem 26:9573–9582
31. Osinga TJ, Linsen BG, Vanbeek WP (1967) J Catal 7:277–279
32. Evans JW, Wainwright MS, Bridgewater AJ, Young DJ (1983) Appl Cat 7:75–83
33. Scholten JJ, KonvalinJa JA (1969) T Faraday Soc 65:2465
34. Bond GC, Namijo SN (1989) J Catal 118:507–510
35. Markmann J, Zimmer P, Birringer R, Chadwick AV (2005) Chem Mater 17:3935–3943
36. Joo J, Yu T, Kim YW, Park HM, Wu FX, Zhang JZ, Hyeon T (2003) J Am Chem Soc 125:6553–6557
37. Stevens R (1986) Zirconia and Zirconia ceramics, 2nd edn. Magnesium Elektron Ltd, United Kingdom
38. Borovinskaya IP, Loryan VE, Grigoryan EA, Salnikova EN, Pershikova NI (1992) Int J SHS 1:131–134
39. Agrell J, Birgersson H, Boutonnet M, Melian-Cabrera I, Navarro RM, Fierro JLG (2003) J Catal 219:389–403
40. Batista J, Pintar A, Mandrino D, Jenko M, Martin V (2001) Appl Cat A Gen 206:113–124
41. Molenbroek AM, Haukka S, Clausen BS (1998) J Phys Chem B 102:10680–10689